Published in final edited form as:
Angew Chem Int Ed Engl. 2008 ; 47(47): 9071–9074. doi:10.1002/anie.200803740.

A Combined NRVS and DFT Study of Fe^{IV}=O Model Complexes: a Diagnostic Method for the Elucidation of Non-Heme Iron Enzyme Intermediates**

Caleb B. Bell III[a], **Shaun D. Wong**[a], **Dr. Yuming Xiao**[b], **Dr. Eric J. Klinker**[c], **Adam L. Tenderholt**[a], **Dr. Matt C. Smith**[b], **Dr. Jan-Uwe Rohde**[c], **Prof Lawrence Que Jr.**[c], **Prof Stephen P. Cramer**[a], and **Prof Edward I. Solomon***,[b]

[a] Edward I Solomon, C. B. Bell III, S. D. Wong and A. L. Tenderholt, Department of Chemistry, Stanford University, Stanford, CA 94305-5080, USA

[b] Y. Xiao, M. C. Smith and S. P. Cramer, Department of Applied Science, University of California, Davis, CA 95616, Physical Biosciences Division, Lawrence Berkeley National Laboratory, Berkeley, CA 94720

[c] E. J. Klinker, J-U. Rohde and Lawrence Que, Jr., Department of Chemistry, University of Minnesota, Minneapolis MN 55455

Abstract

Fe^{IV}=O biomimetic model complexes have been characterized using nuclear vibrational resonance spectroscopy (NRVS). Features and systematic trends in the low energy region reflect equatorial and axial bonding differences that relate to differences in reactivity. These trends have been computationally extended to predict the spectra of putative Fe^{IV}=O intermediates in non-heme iron enzymes and show the utility of the NRVS method for structural insight.

Keywords

iron(IV); NRVS; non-heme iron; Spectroscopic methods; X-ray spectroscopy

Fe^{IV}=O intermediates have been shown to be key catalytic species in a growing number of mononuclear non-heme iron (NHI) enzymes. Various combinations of Mößbauer (Mb), electron-nuclear double resonance, magnetic circular dichroism (MCD), and extended x-ray absorption data exist on these, providing electronic insight and bonding descriptions of the Fe^{IV}=O unit.[1] However information regarding other chemically important features necessary for mechanistic insight (overall structure) is mostly lacking. Resonance Raman (rR) and IR spectroscopy can, in principle, provide such insight, however, due to selection rules, low absorption intensities (NHI species lack the intense Soret band), and other factors, experimental data are limited.[2] Herein, we present vibrational data obtained by nuclear resonance vibrational spectroscopy (NRVS) on three Fe^{IV}=O complexes interpreted via coupling with DFT calculations, with particular focus on understanding the low energy spectral region. The data show systematic trends that provide molecular level insight

**Use of the Advanced Photon Source at Argonne National Laboratory was supported by the U. S. Department of Energy, Office of Science, Office of Basic Energy Sciences, under Contract No. DE-AC02-06CH11357. Financial support of this research was provided by NIH Grants GM65440 (S.P.C), GM33162 (L.Q.), and GM40392 (E.I.S.) and NSF-Biophysics Program Grant MCB-0342807 (E.I.S)). We would like to thank Jjyong Zhao, Wolfgang Sturhahn and the staff at beamline 3-ID for assistance and discussions regarding NRVS.

Fax: (+1) 650-725-0259, E-mail: Edward.Solomon@stanford.edu.

reflecting the Fe^{IV} ligand environment and reactivity. Computationally, these studies are extended to models of the Fe^{IV}=O species in HmaS/HPPD (vide infra) and show that Fe^{IV} species can be experimentally differentiated using NRVS.

The NRVS experiment employs synchrotron radiation tuned to the 14.4 keV ^{57}Fe nuclear Mb transition.[3–5] Inelastic scattering, where phonon annihilation and creation events couple with nuclear excitation, yields the Fe partial vibrational density of states (PVDOS) NRVS spectrum. This is analogous to Stokes and anti-Stokes rR scattering, but NRVS intensity is gained through Fe displacement (ΔFe), via the mode composition factor, and provides selective enhancement of all Fe-core modes with no background.[6] This method has been applied to Fe-S and heme enzymes, nitrogenase and model complexes.[7–16] NRVS data for an Fe^{V}-nitrido complex with a ligand similar to **1** (vide infra) have been reported.[16] However, detailed analysis in the low energy region was complicated by inhomogeneity in the sample.[16]

Fe^{IV}=O (*S* = 1) functional models have been synthesized with 1,4,8,11-tetramethyl-1,4,8,11-tetraazacyclotetradecane (**1**); *N*,*N*-*bis*(2-pyridylmethyl)-*N*-*bis*(2-pyridyl)methylamine (**2**); and *N*-benzyl-*N*,*N*′,*N*′-*tris*(2-pyridylmethyl)-1,2-diaminoethane (**3**) ligands.[17–19] Each complex is 6-coordinate: **1** has an equatorial (eq) ring with tertiary amines and an axial (ax) $NCCH_3$ ligand; **2** has eq pyridines (py) and a tethered ax tertiary amine and **3** is quite rhombic with two tertiary amine and three py ligands. Structures are available for **1** and **2**. Note, **2** and **3** are more reactive than **1** in their ability to H-atom abstract from cyclohexane.[20]

The NRVS data for **1**, **2**, and **3** are shown in Figure 1. Isotope sensitive peaks are observed at 831 (796 in ^{18}O), 820 (788) and 824 (786) cm^{-1}, respectively, that can be assigned as ν_2, the FeO stretch (normal modes in Figure 2).[21,22] Resolution on NRVS energies is 8 cm^{-1}. These correlate well with the calculated energies and isotope shifts, see SI and Figure S2. This mode has been observed only in **1** at 834 by IR and at 839 cm^{-1} by rR, in good agreement with our results.[19,23] The lowerν_2 frequencies for **2** and **3** relative to **1** imply that their FeO bonds are weaker. Excited state MCD data have shown the FeO π bond is stronger in **2** relative to **1** therefore the σ bond must be weaker.[24] This can be rationalized by considering the stronger donation of the eq ligands in **2** (vide infra) which donate into the donut of d_{z2} and compete with the oxo.

Moving down in energy, a weak peak is observed at 653 cm^{-1} in **2** and **3**, while for **1** the next resolvable peak is at 526 cm^{-1}. In **2** and **3** this is assigned, based on DFT calculations, as ν_8, the asymmetric FeN_{eq} stretches. In the calculations, these are shifted to the 450 – 470 cm^{-1} region in **1** and not resolved in the data. In total, 4 modes involve FeN_{eq} stretching (including the NRVS inactive ν_1 and ν_5) and probe eq bonding; the average energy of these sets is 355, 648 and 598 cm^{-1}, respectively. Calculations where the eq ring in **1** is cleaved (**1**′, see SI) show that the average FeN bond length shortens by 0.07 Å, the splitting of the 4 modes decreases and the average increases to 430 cm^{-1}. These results show that the chelate in **1** influences the eq bonding but that the overall strength is determined by the greater σ donation of the py ligands relative to tertiary amines which affects FeO bonding.

Continuing down in energy, the first intense feature is assigned as ν_3 (FeN_{ax} stretch) at 391, 367 and 389 cm^{-1}, in **1**, **2** and **3**, respectively. In the calculations these show variable intensity (bars in Figure 3) and mix with ν_{11}. The resulting ΔFe has both in-plane (ip) and out-of-plane (op) contributions from ν_{11} and ν_3. The ip motion in **1** is restricted due to the chelate, reducing ΔFe, i.e. intensity. In **1**′, ΔFe is restored and ν_3 shifts to 294 cm^{-1}, Figure S4. Calculations where the ax tether is removed in **2** (**2**′, see SI) show that ν_3 is shifted down in energy to 300 cm^{-1}, consistent with a 0.05 Å increase of the FeN_{ax} bond, but the ip and

op ΔFe are preserved. This mode reflects the bond *trans* to the oxo and constraints in the ligand environment.

The remaining two intense features are assigned as $v_{11a/b}$ ($OFeN_{ax}$ bends), which split due to orthogonal differences in the eq ligand environment; ring size in **1**, ax tether in **2** and eq chelate in **3**. The splitting in **3** is 50 cm^{-1} but only ~25 cm^{-1} in **1** and **2** reflecting the contracted eq chelate between a pair of *cis* N's in **3** and affords a probe of rhombic (perpendicular to the FeO) distortion. In **1′**, the most symmetric model, the splitting is 6 cm^{-1}. In **2′** (where, the x and y axes are still inequivalent) the energy positions and splitting are unchanged but the calculated intensity is reduced due to increased N_{ax} motion. The splitting of v_{11} reflects the ligand environment perpendicular to the FeO bond and, combined with high intensity, should provide structural insight for Fe^{IV}=O intermediates.

(4-Hydroxyphenyl)pyruvate dioxygenase (HPPD) and (4-hydroxy)mandelate synthase (HmaS) are NHI enzymes containing the 2 His 1 Glu facial triad and use the same substrate (HPP) but exhibit different reaction mechanisms (electrophilic aromatic attack and H-atom abstraction, respectively) dictated by the orientation of HPP by the protein pocket.[25] The first step in both reactions is decarboxylation of HPP and computational studies on the resultant Fe^{IV}=O site show that two 5C geometries are reasonable: square pyramidal (sqp, **4**) with the oxo in the eq plane and trigional bipyramidal (tbp) with the oxo axial (**5**).[25] Here we determine that NRVS can discriminate between these proposed structures. The calculated PVDOS are shown in Figure 4. The intense peaks at 301 and 424 cm^{-1} in **4** are bends of the $OFeN_{trans}$ unit (*trans* to the oxo) reminiscent of $v_{11a/b}$, where the large splitting arises from loss of the *cis* ligand. Intense peaks are also at 237 and 837 cm^{-1} which involve FeN_{trans} (~v_3) and FeO (~v_2) stretches. For **1**, **2**, and **3**, v_3 was observed at a higher energy relative to v_{11}; the shift to lower energy in **4** is due to the increased effective mass of histidine. The NRVS data of **5** are distinctly different and can be understood considering the normal modes for a tbp complex, Figure S6. The degenerate v_6 and v_7 pairs involve *trans* ax bends and *cis* ML stretches. These are highly mixed in **5** and produce 4 peaks with similar intensity. The *trans* N_{His} stretch (~v_3) is also intense at 257 cm^{-1}. In summary, with the exception of the FeO stretch, the intense modes occur at low energies and, due to the inverse energy dependency of NRVS intensity, are likely to be detectable in enzyme intermediates and afford a mechanism for structural characterization.

Analysis of the ground state NRVS vibrational data coupled with excited state data from previous MCD studies provides detailed bonding descriptions of **1**, **2**, and **3**.[24,26] The increased reactivity of **2** and **3** relative to **1** correlates with the strength of the FeO π bond (oxo p character in the π^* LUMO, the frontier molecular orbital) and is determined by equatorial ligand σ donation. Additionally, the v_3 andv_{11} modes show systematic trends which reflect the ligand environment. Lower energy modes have generally not been used for geometric insight, but in NRVS spectra these are enhanced in intensity relative to higher energy stretches (e.g. characteristic metal ligand modes such as v_{FeO}) and more likely to be detected in intermediates. This study uses these modes for electronic structural insight on Fe^{IV}=O models and computationally evaluates their utility for determination of active site structure in NHI enzyme intermediates.

Experimental Section

Samples prepared as previously described.[17,18] NRVS was collected on beamline 3-ID at Advance Photon Source on multiple visits.[6,7,27] Spectra were collected from −25 and 125 meV in 0.25 meV steps. 5 to 12 scans were averaged and normalized from which the PVDOS was generated using the PHOENIX program.[28] Spin-unrestricted DFT calculations were performed using Gaussian 03 (see SI).

References

1. See Fe(IV) special edition of *J Inorg Biochem* 2006, *100*, and references therein.
2. Proshlyakov DA, Henshaw TF, Monterosso GR, Ryle MJ, Hausinger RP. J Am Chem Soc. 2004; 126:1022. [PubMed: 14746461]
3. Sturhahn W. J Phys Condens Matter. 2004; 16:S497.
4. Scheidt WR, Durbin SM, Sage JT. J Inorg Biochem. 2005; 99:60. [PubMed: 15598492]
5. Rüffer R, Chumakov AI. Hyperfine Interactions. 2000; 128:255.
6. Alp EE, Mooney TM, Toellner T, Sturhahn W. Hyperfine Interactions. 1994; 90:323.
7. Xiao Y, Wang H, George SJ, Smith MC, Adams MW, Jenney FE Jr, Sturhahn W, Alp EE, Zhao J, Yoda Y, Dey A, Solomon EI, Cramer SP. J Am Chem Soc. 2005; 127:14596. [PubMed: 16231912]
8. Leu BM, Zgierski MZ, Wyllie GR, Scheidt WR, Sturhahn W, Alp EE, Durbin SM, Sage JT. J Am Chem Soc. 2004; 126:4211. [PubMed: 15053610]
9. Achterhold K, Sturhahn W, Alp EE, Parak FG. Hyperfine Interactions. 2002; 141–142:3.
10. Xiao Y, Tan ML, Ichiye T, Wang H, Guo Y, Smith MC, Meyer J, Sturhahn W, Alp EE, Zhao J, Yoda Y, Cramer SP. Biochemistry. 2008
11. Xiao Y, Fisher K, Smith MC, Newton WE, Case DA, George SJ, Wang H, Sturhahn W, Alp EE, Zhao J, Yoda Y, Cramer SP. J Am Chem Soc. 2006; 128:7608. [PubMed: 16756317]
12. Rai BK, Durbin SM, Prohofsky EW, Sage JT, Wyllie GR, Scheidt WR, Sturhahn W, Alp EE. Biophys J. 2002; 82:2951. [PubMed: 12023218]
13. Rai BK, Durbin SM, Prohofsky EW, Sage JT, Ellison MK, Roth A, Scheidt WR, Sturhahn W, Alp EE. J Am Chem Soc. 2003; 125:6927. [PubMed: 12783545]
14. Rai BK, Prohofsky EW, Durbin SM. J Phys Chem B Condens Matter Mater Surf Interfaces Biophys. 2005; 109:18983. [PubMed: 16853444]
15. Cramer S, Xiao Y, Wang H, Guo Y, Smith M. Hyperfine Interactions. 2006; 170:47.
16. Petrenko T, DeBeer George S, Aliaga-Alcalde N, Bill E, Mienert B, Xiao Y, Guo Y, Sturhahn W, Cramer SP, Wieghardt K, Neese F. J Am Chem Soc. 2007; 129:11053. [PubMed: 17711275]
17. Klinker EJ, Kaizer J, Brennessel WW, Woodrum NL, Cramer CJ, Que L Jr. Angew Chem Int Ed. 2005; 44:3690.
18. Rohde JU, Torelli S, Shan X, Lim MH, Klinker EJ, Kaizer J, Chen K, Nam W, Que L. Angew Chem Int Ed, Vol. 126; 2004:16750.
19. Rohde JU, In JH, Lim MH, Brennessel WW, Bukowski MR, Stubna A, Münck E, Nam W, Que L Jr. Science. 2003; 299:1037. [PubMed: 12586936]
20. Kaizer J, Klinker EJ, Oh NY, Rohde JU, Song WJ, Stubna A, Kim J, Munck E, Nam W, Que L. J Am Chem Soc. 2004; 126:472. [PubMed: 14719937]
21. Preetz W, Ruf D, Tensfeldt D. Zeitschrift Fur Naturforschung Section B-a Journal of Chemical Sciences. 1984; 39:1100.
22. Nakamoto, K. Infrared and Raman Spectra of Inorganic and Coordination Compounds. John Wiley & Sons, Inc; New York: 1997.
23. Jackson TA, Rohde JU, Seo MS, Sastri CV, DeHont R, Ohta T, Kitagawa T, Munck E, Que L Jr. J Am Chem Soc. 2008; 130 In press.
24. Decker A, Rohde JU, Que L Jr, Solomon EI. J Am Chem Soc. 2004; 126:5378. [PubMed: 15113207]
25. Neidig ML, Decker A, Choroba OW, Huang F, Kavana M, Moran GR, Spencer JB, Solomon EI. Proc Natl Acad Sci U S A. 2006; 103:12966. [PubMed: 16920789]
26. Decker A, Rohde JU, Klinker EJ, Wong SD, Que L Jr, Solomon EI. J Am Chem Soc. 2007; 129:15983. [PubMed: 18052249]
27. Sturhahn W. Hyperfine Interactions. 1995; 95:6.
28. Sturhahn W. Hyperfine Interactions. 2000; 125:149.

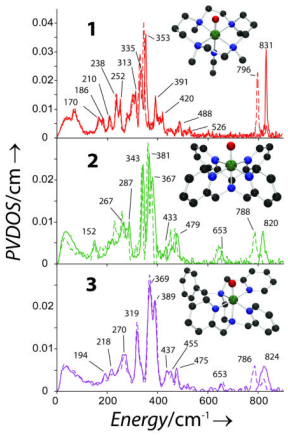

Figure 1.
NRVS PVDOS for **1**, **2** and **3** with ^{16}O (solid lines) and ^{18}O (dotted lines), insets show the 3D structures of complexes.

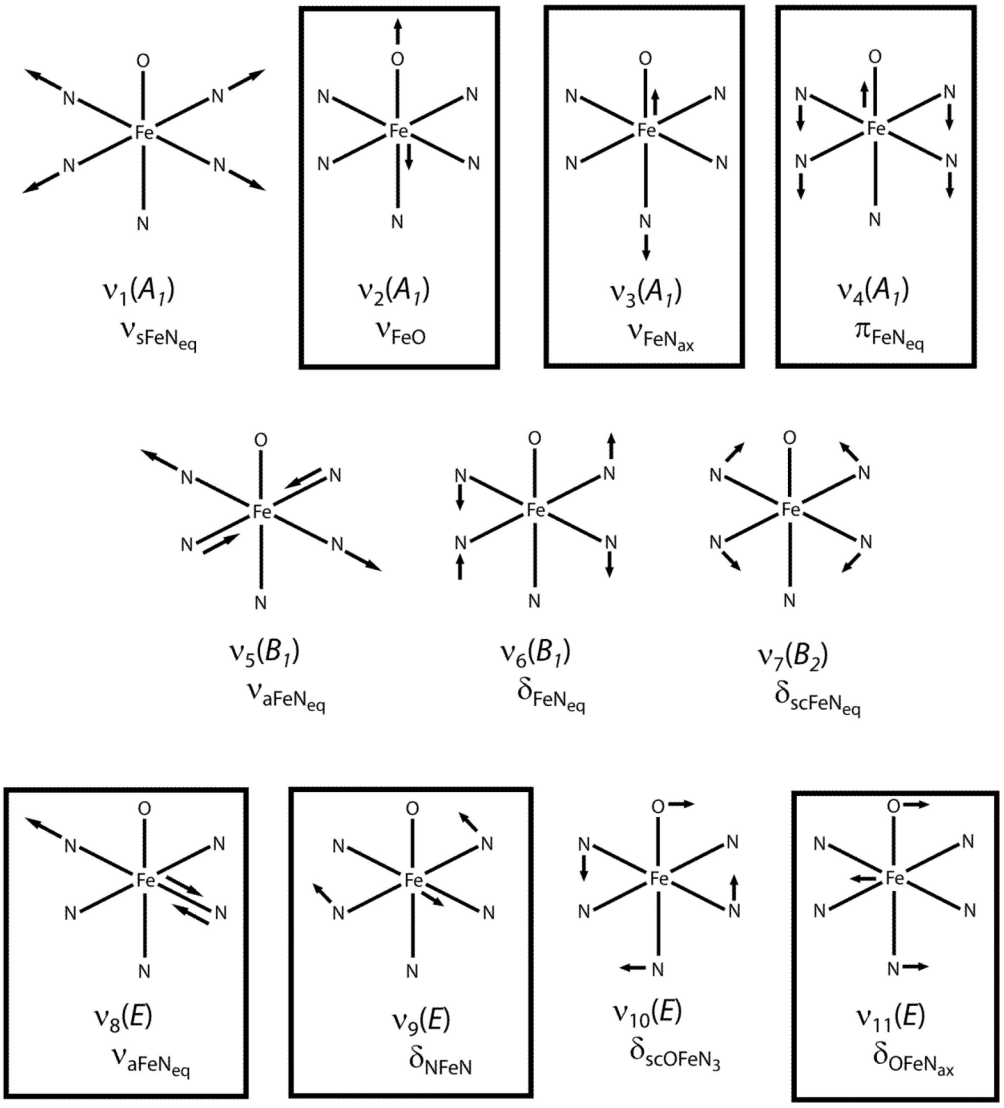

Figure 2.
Normal modes for C_{4v} complexes adapted from ref.[21] Modes with ΔFe are boxed. Nomenclature follows Nakamoto.[22]

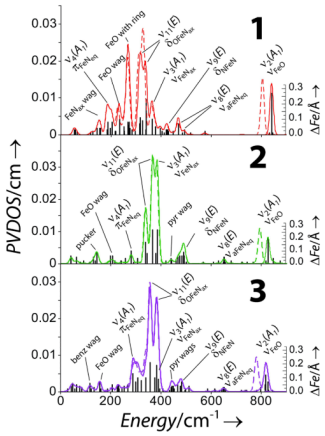

Figure 3.
DFT calculated NRVS PVDOS for **1**, **2** and **3** (^{16}O (solid lines) and ^{18}O (dotted lines)) with ΔFe included as bars.

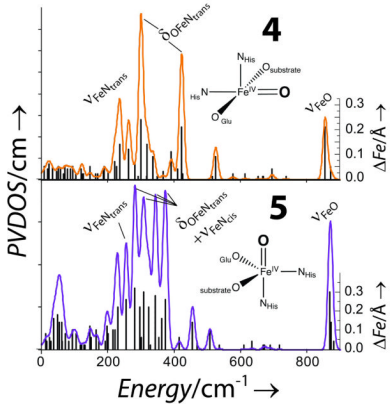

Figure 4.
DFT calculated NRVS PVDOS for **4** and **5** with ΔFe.